

# Flexible Mesh Segmentation through Integration of Geometric and Topological Features of Reeb Graphs

F. Beguet, S. Lanquetin and R. Raffin

University of Burgundy, LIB, EA7534

---

## Abstract

Mesh segmentation represents a crucial task in computer graphics and geometric analysis, with diverse applications spanning texture mapping, animation, and beyond. This paper introduces an innovative Reeb graph-based mesh segmentation method that seamlessly integrates geometric and topological features to achieve flexible and robust segmentation results. The proposed approach encompasses three primary phases. First, an enhanced topological skeleton construction efficiently captures the Reeb graph structure while preserving degenerate critical points. Second, a topological simplification process employing critical point cancellation reduces graph complexity while maintaining essential shape features and correspondences. Finally, a region growing algorithm leverages both Reeb graph adjacency and mesh vertex connectivity to generate contiguous, semantically meaningful segments.

The presented method exhibits computational efficiency, achieving a complexity of  $O(n \log n)$  for a mesh containing  $n$  vertices. Its versatility and effectiveness are validated through application to both local geometry-based segmentation using the Shape Index and part-based decomposition utilizing the Shape Diameter Function. This flexible framework establishes a solid foundation for advanced analysis and applications across various domains, offering new possibilities for mesh processing and understanding.

## CCS Concepts

• **Computing methodologies** → 3D Mesh Segmentation; Reeb Graph; Discrete Morse theory; Shape Index; Shape Diameter Function;

---

## 1. Introduction

Mesh segmentation plays a crucial role in computer graphics and geometric analysis, serving various purposes across applications such as texture mapping [SWG\*03], shape matching [DGG03], shape modeling [FKS\*04], mesh compression [KG00], mesh simplification [?], and animation [YLX\*16]. The primary aim is to segment complex 3D mesh models into continuous and relevant parts according to the user's interests. However, segmentation algorithms face challenges in accurately and efficiently dividing such models due to intricate geometric structures, irregularities, and a wide range of shapes, scales, and topologies. The presence of noisy or incomplete data further complicates segmentation accuracy. Balancing between over-segmentation and under-segmentation, avoiding excessive fragmentation or merging of regions, is a critical challenge. Ensuring robustness across different object types, such as organic and man-made, remains an ongoing concern. Addressing these challenges is vital for advancing mesh segmentation algorithms and enhancing their practical applications.

### 1.1. Related works

In this paper, we focus mainly on highlighting two primary categories of approaches: those falling under the surface-based

paradigm and those classified as skeleton-based methods. Surface-based segmentation involves partitioning a surface mesh into distinct segments or regions, composed of interconnected facets sharing geometric similarities such as convexity or curvature. On the other hand, skeleton-based approaches, also known as skeletonization, aim to build a connected linear representation of a mesh that encapsulates the essential structural attributes of the supplied mesh by tracing a path to its boundaries. It should be noted that there is a substantial literature evaluating various segmentation methods for meshes, with citations such as [AKM\*06, APP\*07, Sha08, TPT15, RMG18].

#### 1.1.1. Surface-based segmentation

Surface-based mesh segmentation algorithms focus on geometric information, such as curvature or saliency, to divide the surface mesh into distinct segments. These methods can be grouped into three sub-categories: region-growing, clustering and boundary segmentation.

**Region-growing** methods [ZTS02, ZH04, LW08, ZLXH08, BAT12], inspired by polyhedral surface decomposition [CDST95], progressively enlarge initial seed regions guided by predetermined criteria. This approach enables the formation of segments align-

ing closely with the mesh’s geometric properties. There are also alternative methods [MW98, Kos03, BPVR11] draw from *Watershed* image analysis [Beu92], partitioning the mesh into *catchment basins* for localized segmentation. However, the efficacy of region-growing relies heavily on seed selection quality and appropriate stopping criteria, as inadequate choices can lead to over or under-segmentation, implying additional merging steps to address potential issues.

**Clustering** methods [STK02, LHMR08, SSCO08], initially rooted in the K-means algorithm [Llo82], involve selecting representative seeds to create segments. K-means clustering-based approaches face challenges in determining the optimal number of segments, often addressed through spectral information integration [LZ04, FSKR11, ZZWC12]. **Hierarchical clustering** techniques, including top-down [KT03, ZL\*05, LZHM06, PSG\*06, LZ07, ZLG\*15] and bottom-up [AFS06] approaches, organize segments hierarchically, enabling multi-level analysis. While top-down decomposition halts based on minimum size, maximum depth, or part limit criteria, bottom-up clustering evaluates merging pairs based on cost, forming a hierarchical cluster structure. The selection of a meaningful merging criterion is critical, as to region-growing methods. The main difficulty with hierarchical clustering is knowing when to halt the segmentation process to avoid excessive subdivision. Furthermore, these techniques can be computationally costly, especially on large meshes, and the number of generating clusters is rarely known ahead of time.

**Boundary segmentation** methods aim to identify the boundary or contour of each segment, typically composed of connected edges and vertices. These methods align with Hoffman’s theory [HS97], suggesting that human vision discerns object boundaries by tracking negative minima of principal curvatures. Techniques employed include identifying shortest paths fulfilling predefined cost functions [LLS\*05], generating multiple segmentations to determine suitability [GF08], searching for isolines of scalar functions [AZC\*11, WLAT14], or applying edge-based segmentation methods common in image analysis [RMG15]. Challenges in these methods revolve around detecting multiple borders, finding effective closed boundaries, and determining the number of regions automatically [RMG18].

### 1.1.2. Skeleton-based segmentation

Skeleton-based mesh segmentation algorithms focus on the topological information of the mesh, building a 1D structure that simplifies the representation of the object’s shape. This representation can be constructed using three distinct methods: medial axis transform, geometric contraction and Reeb graphs.

The **Medial Axis Transform**, introduced by [Blu67], is a key concept in computational geometry and computer graphics. It represents the path traced by centers of maximally inscribed balls touching a 3D mesh. Various algorithms [BA92, ACK01] utilize Voronoi diagrams, while [WML\*06] detects maximum spheres that don’t intersect the surface. The complexity of constructing the medial axis poses a significant challenge, especially with concave or irregular shapes. Consequently, medial axis-based segmentation primarily focuses on elongated or tubular shapes to attenuate these challenges [MPS\*04, MPS06, SLSK07, CSM07].

**Geometric contraction** is a process aimed at reducing a shape to its skeletal representation, typically achieved through volumetric or mesh contraction methods. Volumetric techniques [Pud98, CCZ07, BKS01], prevalent in skeleton extraction, rely on discrete volumetric representations of surface meshes, where voxel resolution affects feature delineation precision. In contrast, Mesh contraction methods [LWTH01, ATC\*08] directly operate on the surface, involving iterative smoothing and contraction steps to transform it into a near-zero volume mesh while preserving topology. However, these methods may result in an unconnected skeleton, often requiring additional reconstruction steps.

**Reeb graphs**, originating from Morse theory [Mil63], provide a fundamental framework for characterizing spaces by analyzing real functions defined on them. These graphs reveal significant divisions corresponding to distinct regions or components within a mesh, influenced by the choice of scalar function, with the skeleton generated from the function’s isolines. Initially, height functions were common for Reeb graph computation and mesh segmentation [SKK91, XSW03], but their lack of rotational invariance led to varying results. As a result, Reeb graph-based segmentation methods have shifted towards using geodesic distance [TVD07, BDBP09] due to its affine transformation invariance and robustness against noise and deformations. However, computing geodesic distance is computationally intensive and often involves selecting a subset of surface vertices. Curvature-based estimation functions are less common for mesh segmentation [MP02] but exhibit affine transformation and topological change invariance, even if they have noise problems. Strategies to mitigate this include adapting the curvature calculation radius for smoother results or applying filtering approaches to the function.

## 1.2. Overview and paper organization

In summary, surface-based segmentation methods utilize geometric mesh information to create meaningful segments but often result in excessive subdivisions, necessitating merging processes. These methods are heavily reliant on predefined criteria, limiting adaptability between them, and determining the optimal number of segments poses a challenge, typically addressed through semi-automatic or threshold-based automated approaches. Conversely, skeleton-based segmentation methods automate the process and excel in segmenting tubular or articulated meshes due to the topological information within the skeleton, though they struggle with mechanical parts and handcrafted objects. Although Reeb graphs are considered skeleton-based structures, the use of functions based on local geometric information, such as curvature, can give results close to surface-based methods without the need to predefine a number of segments. However, this produces noisy graphs that pose problems for direct mesh segmentation, unlike previous studies that relied on height or geodesic functions [XSW03, TVD07, BDBP09]. Additionally, the vertices set between two saddle nodes of the graph does not consistently form a contiguous discrete region suitable for segmentation, a point we address in Section 3.1.

In this paper, we present a new mesh segmentation method using Reeb graphs derived from any scalar function, addressing noisy graphs and resolving issues of discrete non-continuous regions between saddle nodes. The flexibility of scalar function selection al-

allows users to adapt the observation of surface geometry to the requirements of the application, whether local or global descriptions are involved. This versatility makes our method suitable for a variety of object recognition and shape analysis tasks. The use of Reeb graphs as an intermediate representation offers a significant computational advantage, improving operational efficiency over conventional surface-based segmentation methods applied directly on the entire mesh dataset. In addition, it facilitates the rapid generation of multiple segmentations from a single Reeb graph, underlining its usefulness and adaptability in advanced mesh analysis scenarios.

The paper is structured as follows: Section 2 provides the theoretical background of Morse theory and Reeb graphs. Section 3 presents the proposed method in three steps: Reeb graph construction using enhanced topological skeletons, topological simplification through critical point cancellation, and region growing that ensures continuous segmentation. Section 4 demonstrates our approach through experiments with Shape Diameter Function and Shape Index. Finally, Section 5 concludes with a discussion of applications and future directions.

## 2. Theoretical background

Morse theory and Reeb graphs are mathematical tools used in the study of topological spaces and the analysis of functions defined on them. These concepts provide a deeper understanding of the intrinsic geometry and structure of these spaces by uncovering critical points, connecting them, and revealing essential topological features.

### 2.1. Morse Theory

Morse theory establishes a connection between the differential geometry of a surface and its topology. When applied to a manifold  $M$  alongside a real-valued function  $f$  defined on it, it describes the connectivity of the shape using a representation based on the set of points where the function's gradient nullifies. Termed as *critical points* of the function, these points fall into three distinct classes: *minimum*, *maximum*, and *saddle*. The remaining points of  $f$  are referred to as *regular points*.

Let  $p$  be a point of  $M$ , its coordinates  $(u, v)$  and  $H_f(p)$  the Hessian matrix corresponding:

$$H_f(p) := \begin{bmatrix} \frac{\partial^2 f}{\partial u^2}(p) & \frac{\partial^2 f}{\partial u \partial v}(p) \\ \frac{\partial^2 f}{\partial v \partial u}(p) & \frac{\partial^2 f}{\partial v^2}(p) \end{bmatrix} \quad (1)$$

if  $\det(H_f(p)) \neq 0$  then  $p$  is a *non-degenerate critical point* and the *Morse index*  $k$  of  $p$  is obtained by counting the number of negative eigenvalues of the Hessian matrix. For a manifold of dimension 2, the index  $k$  of such a point can be used to determine its nature:

- if  $k = 0$ ,  $p$  is a minimum point;
- if  $k = 1$ ,  $p$  is a saddle point;
- if  $k = 2$ ,  $p$  is a maximum point.

While continuous Morse theory offers a comprehensive theoretical basis for topological analysis, its practical implementation for

real-world data and computational tasks can be prohibitively expensive. Conversely, discrete Morse theory, introduced by [Ban70], presents a more computationally accessible option, as it approximates topological structures using discrete data and streamlines the analysis procedure. In the remainder of this section, we will explore the principles and advantages of discrete Morse theory, viewing it as an extension of continuous Morse theory.

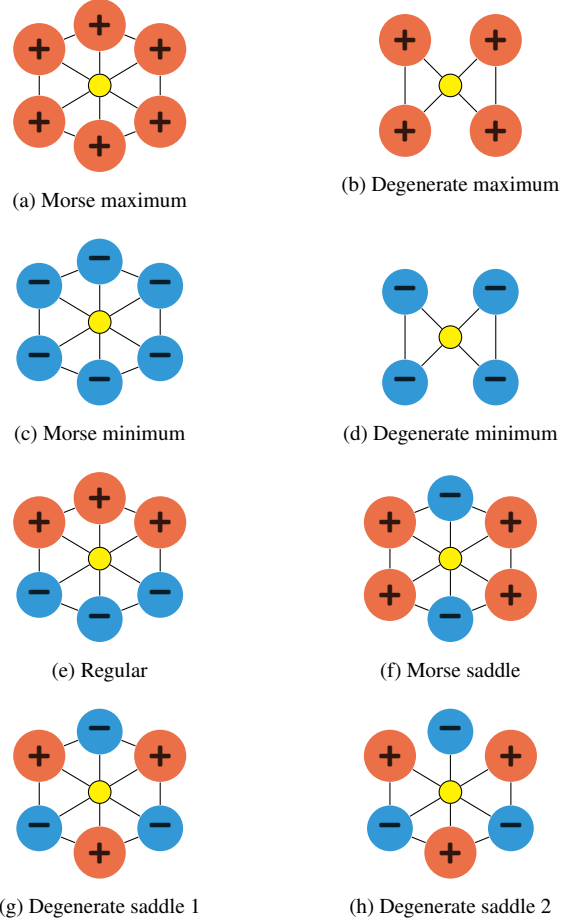


Figure 1: Classification of vertex configurations in discrete Morse theory.

Let  $v$  be a vertex on a 2-manifold surface  $S$  and  $f$  be a scalar function defined on  $S$ :

- The *superior link*  $Li^+(S, v, f)$  of vertex  $v$  is defined as the set of all vertices  $v_i$  in the neighborhood  $N(v)$  where  $f(v_i) > f(v)$ , together with all edges  $e_{ij}$  connecting pairs of these vertices. We denote by  $|Li^+(S, v, f)|$  the number of connected components in the resulting subgraph.
- the *inferior link*  $Li^-(S, v, f)$  follows an analogous definition for vertices where  $f(v_i) < f(v)$

To handle ambiguous cases where adjacent vertices have identical values, [NGH04] proposed an approach which draws from Conley index theory. This theoretical framework, introduced by [MM02], enables critical region classification in vector fields

through boundary value analysis. Under this approach, we treat any set of adjacent vertices with equal values as a single vertex.

Based on these definitions, we classify each vertex  $v$  on surface  $S$  into one of the following categories:

- let  $|Li^+(S, v, f)| = k$  and  $|Li^-(S, v, f)| = 0$  with  $k > 0$ . If  $k = 1$ , then  $v$  is a Morse maximum (figure 1a), else if  $m > 1$ ,  $v$  is a degenerate maximum (figure 1b);
- let  $|Li^+(S, v, f)| = 0$  and  $|Li^-(S, v, f)| = k$  with  $k > 0$ . If  $k = 1$ , then  $v$  is a Morse minimum (figure 1c), else if  $k > 1$ ,  $v$  is a degenerate minimum (figure 1d);
- let  $|Li^+(S, v, f)| = |Li^-(S, v, f)| = k$  with  $k > 0$ . If  $k = 1$ , then  $v$  is a regular vertex (figure 1e), else if  $k = 2$ , then  $v$  is a Morse saddle vertex (figure 1f). When  $k > 2$ , we define the multiplicity  $m$  of the saddle point as  $m = (k - 1)$ , representing the number of level set crossings at  $v$ . Such vertices are classified as degenerate saddle points (see figures 1g and 1h). Topologically, a degenerate saddle with multiplicity  $m$  can be interpreted as the merging of  $m$  simple Morse saddles, resulting in more complex level set behavior at these critical points.

The classification of critical points through discrete Morse theory provides essential local differential properties of the surface. However, a complete topological characterization necessitates understanding the relationships between these critical points within the global structure of the manifold.

## 2.2. Reeb Graph

The Reeb graph formalism, introduced by Milnor [Mil63], provides a rigorous mathematical framework for analyzing the topological structure of a manifold through the evolution of level sets of a smooth function. This construction establishes a systematic approach to encoding the connectivity between critical points by tracking the behavior of level sets as the function value varies. When applied in conjunction with discrete Morse theory, the analysis of these level set transformations yields a graph structure that captures the fundamental topological features of the surface.

To formally analyze level sets on triangulated surfaces, we first define how scalar functions extend from vertices to the entire surface through linear interpolation. A piecewise linear function  $f^* : S \rightarrow \mathbb{R}$  is defined as the extension of a scalar function  $f : V \rightarrow \mathbb{R}$  applied to the set of vertices  $V$  of a triangulated surface  $S$  by linear interpolation:

$$f^*(p) := \sum_{v_i \in \sigma} \lambda_i f(v_i), \quad \forall p \in \sigma \in S \quad (2)$$

where  $\lambda_i$  are the barycentric coordinates of point  $p$  in triangle  $\sigma$ , satisfying:  $\sum_i \lambda_i = 1$  and  $\lambda_i \geq 0$  for all  $i$

A  $l$  level set of  $f^*$  on  $S$  consists of all the points  $x$  such as  $f^*(x) = l$ . The connected components of a level set are called *isolines*. Given  $v$  a vertex of  $S$ , the nature of  $v$  can be used to determine the behaviour of the isoline of the level set passing through this vertex :

- if  $v$  is a minimum or maximum vertex, then the isoline of the level set degenerates to a point;

- if  $v$  is a regular vertex, then the isoline of the level set is a closed line, as illustrated in Figure 2a;
- if  $v$  is a saddle vertex with a multiplicity  $m$ , then the isoline of the level set is the union of  $m$  closed lines intersecting at  $v$ , as shown in Figure 2b.

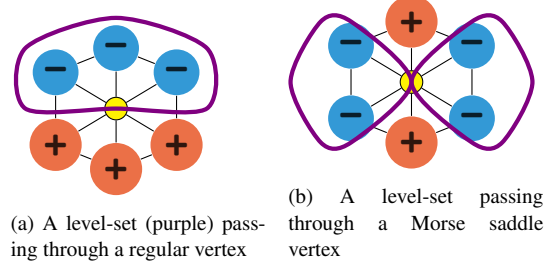


Figure 2: Level-set configurations: regular vertex (a) and Morse saddle vertex (b) with their isolines

Let  $f_{min}^*$  and  $f_{max}^*$  denote the minimum and maximum values of  $f^*$  across the surface. The interval including all values of  $l$  in the interval  $[f_{min}^*, f_{max}^*]$  can be assigned a topology. The isolines created by critical points (maximum, minimum, and saddle) are recognized as nodes within a graph, while isolines originating from regular points are considered as vertices of edges in the graph. To put it more formally, the Reeb graph of  $f^*$  is the quotient space defined by the equivalence relation:

$$(x, f^*(x)) \sim (y, f^*(y)) \Leftrightarrow f^*(x) = f^*(y) = l \quad (3)$$

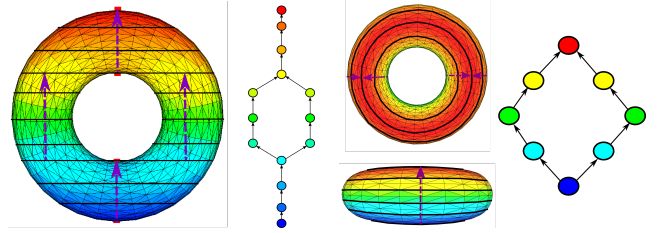


Figure 3: Level sets and Reeb graphs of a torus, comparing Morse (a) and non-Morse (b) height functions

The construction and structure of Reeb graphs can be illustrated through the analysis of scalar functions on a torus. Figure 3 demonstrates two distinct height functions that generate different Reeb graph configurations. In Figure 3a, a height function in the Y-direction yields four non-degenerate critical points: a minimum (blue), a maximum (red), and two saddle points (cyan and yellow). Such a function, containing only non-degenerate critical points, is classified as a Morse function. Its Reeb graph forms a cycle, reflecting the fundamental topology of the torus through the connectivity of its critical points. Conversely, Figure 3b presents a height function in the Z direction that exhibits degenerate critical points at its extremities. This non-Morse function, known as a

round function, generates continuous circles of maxima and minima rather than isolated critical points. The resulting Reeb graph displays a distinct topological structure where the vertical distribution of nodes corresponds to height values, with degenerate critical points appearing at the extremal nodes. These examples highlight both the dependence of Reeb graph structure on the chosen scalar function and the significance of degenerate critical points in Reeb graph analysis and manipulation.

### 3. Methodology

While Reeb graphs provide powerful tools for shape analysis, their direct application to mesh segmentation presents several computational challenges, particularly when using geometric scalar functions. We address these challenges through a three-phase segmentation algorithm:

1. **Reeb graph construction:** The algorithm computes a Reeb graph from a user-defined scalar function on the mesh, implementing an enhanced topological skeleton approach for efficient processing.
2. **Topological Simplification:** A critical point cancellation procedure processes both simple and degenerate critical points to reduce graph complexity while maintaining topological consistency.
3. **Region Generation:** A region-growing algorithm propagates from critical points using both Reeb graph adjacency and mesh vertex connectivity to ensure contiguous segments.

#### 3.1. Reeb graph construction

The construction of a Reeb graph requires careful consideration of how to effectively capture the topological structure encoded by the level sets of a scalar function defined on the mesh. For mesh segmentation applications, this construction must balance computational efficiency, topological accuracy, and robustness to noise. Several approaches have been developed to address these challenges, each with distinct trade-offs.

The **level set diagram** approach [LV99, HA03] tracks the evolution of level set components by sampling the scalar function at discrete intervals. Although initially designed for genus-zero surfaces, this method has been extended to handle more complex topologies. However, its effectiveness heavily depends on the choice of sampling parameters, which can affect both accuracy and computational cost.

The **extended Reeb graph** method [BFS00, ABS03] constructs critical regions by analyzing connected components between successive level sets. While this approach provides explicit topological assessment, its reliance on fixed interval sizes can lead to missed features, particularly in regions where the function gradient varies significantly or where multiple critical points lie within the same interval.

The **multi-resolution Reeb graph** approach [HSKK01] attempts to address sampling limitations by analyzing the scalar function at multiple scales. This hierarchical strategy captures features at various levels of detail but may lack the theoretical guarantees

needed for robust topological analysis, particularly when dealing with degenerate critical points.

The **enhanced topological skeleton** method [TVD09, BP12, Par12] takes a fundamentally different approach by leveraging discrete contours to approximate level sets (Figure 4). This method directly analyzes the behavior of level sets in the neighborhood of each vertex, using upper and lower discrete contours to characterize critical points according to discrete Morse theory. The Reeb graph is then constructed as an adjacency graph where nodes represent discrete contours, and edges connect adjacent discrete contours on the mesh. As illustrated in Figure 4, a level set (purple) passing through a regular point (yellow) is bounded by discrete contours above (red) and below (blue), providing a complete characterization of the local topology without requiring parameter tuning.

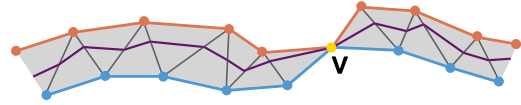


Figure 4: Strip of triangles surrounding the level line (purple) of a regular point (yellow). Discrete contours at the top (red) and bottom (blue) represent this level line.

Given these considerations, we use the enhanced topological skeleton approach, specifically following the methodology of [Par12]. This choice is motivated by several key advantages:

1. Parameter independence, eliminating the need for arbitrary sampling choices
2. Direct alignment with discrete Morse theory, enabling robust handling of degenerate critical points
3. Optimal computational complexity of  $O(n \log n)$  for a mesh with  $n$  vertices
4. Natural extension to higher-dimensional manifolds without modification to the core algorithm

However, this approach also presents certain challenges. The method exhibits high sensitivity to local variations in the scalar function and captures fine-scale variations, including those induced by noise or minor geometric fluctuations. This results in a Reeb graph that, while topologically accurate, may contain numerous critical points that do not represent significant shape features.

These advantages make the enhanced topological skeleton approach particularly suitable for mesh segmentation applications. However, practical implementation requires careful consideration of data structures and algorithmic design.

The graph representation is optimized by storing only critical nodes and their connections. Regular vertices are maintained as sorted lists along the edges between critical nodes, preserving the full topology. Specifically, for each edge  $e$  connecting critical points  $c_1$  and  $c_2$ , we maintain an ordered sequence  $v_1, \dots, v_k$  of regular vertices such that:  $f(c_1) \leq f(v_1) \leq \dots \leq f(v_k) \leq f(c_2)$  or  $f(c_1) \geq f(v_1) \geq \dots \geq f(v_k) \geq f(c_2)$

A key feature of the proposed approach is the preservation of degenerate critical points in their compact form, rather than unfolding

them into multiple simple critical points. This design choice is crucial for mesh segmentation, as it maintains a direct one-to-one correspondence between critical nodes and mesh vertices. Each critical point, whether simple or degenerate, corresponds to exactly one vertex in the mesh, providing a natural seed point for segment propagation. This correspondence would be lost if degenerate critical points were unfolded, potentially creating artificial critical points without direct geometric counterparts in the mesh.

The characteristics of the initial Reeb graph, particularly its sensitivity to local variations and treatment of degenerate critical points, motivate our subsequent critical point cancellation phase. This phase must carefully handle both simple and degenerate critical points while preserving the essential topological structure of the shape and maintaining the crucial vertex correspondence needed for segmentation.

### 3.2. Topological simplification

Geometric scalar functions often produce Reeb graphs with numerous critical points that reflect local surface variations rather than significant shape features. While these points accurately represent the local topology, they can complicate subsequent analysis and segmentation tasks. While Morse theory traditionally addresses this through critical point cancellation - a process that eliminates pairs of critical points while preserving topological structure - this classical approach requires adaptation for Reeb graphs containing degenerate critical points identified through discrete Morse theory. The proposed cancellation algorithm processes both simple and degenerate critical points while maintaining two essential properties: the direct correspondence between graph elements and mesh vertices, and the preservation of global topological features.

The topological simplification process evaluates Reeb graph edges using complementary metrics that assess both local geometric properties and global topological significance. This evaluation identifies non-essential features while preserving the graph's fundamental structure. Multiple edges between node pairs are not considered as they represent significant topological features such as cycles, which characterize essential shape properties of the underlying mesh including handles and tunnels.

For any edge  $e$  connecting nodes  $n_1$  and  $n_2$ , an area ratio  $R_a(e)$  measures regional significance while maintaining scale invariance:

$$R_a(e) = \frac{\sum_{v \in V(e)} A(v) + \sum_{v \in N(e)} \frac{A(v)}{\deg(v)}}{A_{total}} \quad (4)$$

where  $V(e)$  represents the set of vertices along edge  $e$ ,  $N(e)$  comprises vertices in nodes  $n_1$  and  $n_2$ ,  $A(v)$  denotes the area associated with vertex  $v$ ,  $\deg(v)$  indicates the number of edges incident to the node containing  $v$ , and  $A_{total}$  represents the total surface area of the mesh.

A separation metric  $S(e)$  complements this geometric measure by quantifying topological significance through the scalar value difference between endpoint nodes:

$$S(e) = |f(n_1) - f(n_2)| \quad (5)$$

The process employs user-defined thresholds  $\tau_a$  and  $\tau_s$  to identify

candidate edges for cancellation:

$$\text{isCandidate}(e) = \begin{cases} \text{true} & \text{if } R_a(e) < \tau_a \text{ or } S(e) < \tau_s \\ \text{false} & \text{otherwise} \end{cases} \quad (6)$$

The separation metric establishes connections with persistence-based methodologies through its quantification of topological feature significance via scalar value differences between critical points. The integration of geometric considerations through the area ratio metric extends the theoretical framework beyond traditional persistence analysis, enabling a more comprehensive evaluation of feature importance that considers both topological persistence and spatial extent. This combined approach provides a robust foundation for distinguishing between significant shape characteristics and noise-induced variations in the scalar field.

The algorithm manages candidate edges through a priority queue data structure, where edges are ordered by their separation metric values. This organization ensures efficient processing of edges in ascending order of their separation values, prioritizing the merging of features with similar scalar field values.

For each candidate edge, the algorithm applies one of two fundamental operations based on the nature of its endpoint nodes.

The first operation addresses saddle-extremum pairs. When processing an edge connecting a saddle node to an extremum node, the algorithm eliminates both the edge and the extremum node while preserving the saddle node. This operation maintains the topological significance of the saddle point while removing less significant extrema. The scalar values of vertices associated with the removed extremum and its incident edges are adjusted to match that of the preserved saddle node.

The second operation handles extrema-extrema pairs. For edges connecting two extrema, the algorithm replaces both nodes and the connecting edge with a new node. The scalar value of this new node represents the median of the original nodes' values, effectively smoothing the scalar function along the affected branch of the graph. Additional edges previously connected to either extremum are reconnected to the new node.

Both operations require careful management of the graph structure to maintain topological consistency:

- First, all vertices associated with removed nodes, along with vertices on their incident edges whose scalar values fall within the range defined by the cancelled nodes, must be reassigned the scalar value of either the preserved node (in saddle-extremum cancellation) or the newly created node (in extrema-extrema cancellation). This value reassignment ensures continuity in the scalar function across the affected region.
- Second, when removing extrema nodes, any additional edges that were originally connected to these nodes must be carefully reconnected to the preserved or newly created node. This reconnection preserves the graph's connectivity while maintaining the proper relationships between remaining critical points.
- Third, the algorithm monitors the local topology around preserved nodes after edge modifications. If a preserved node attains regular characteristics - specifically, when it has exactly one incoming and one outgoing edge - it is removed from the set



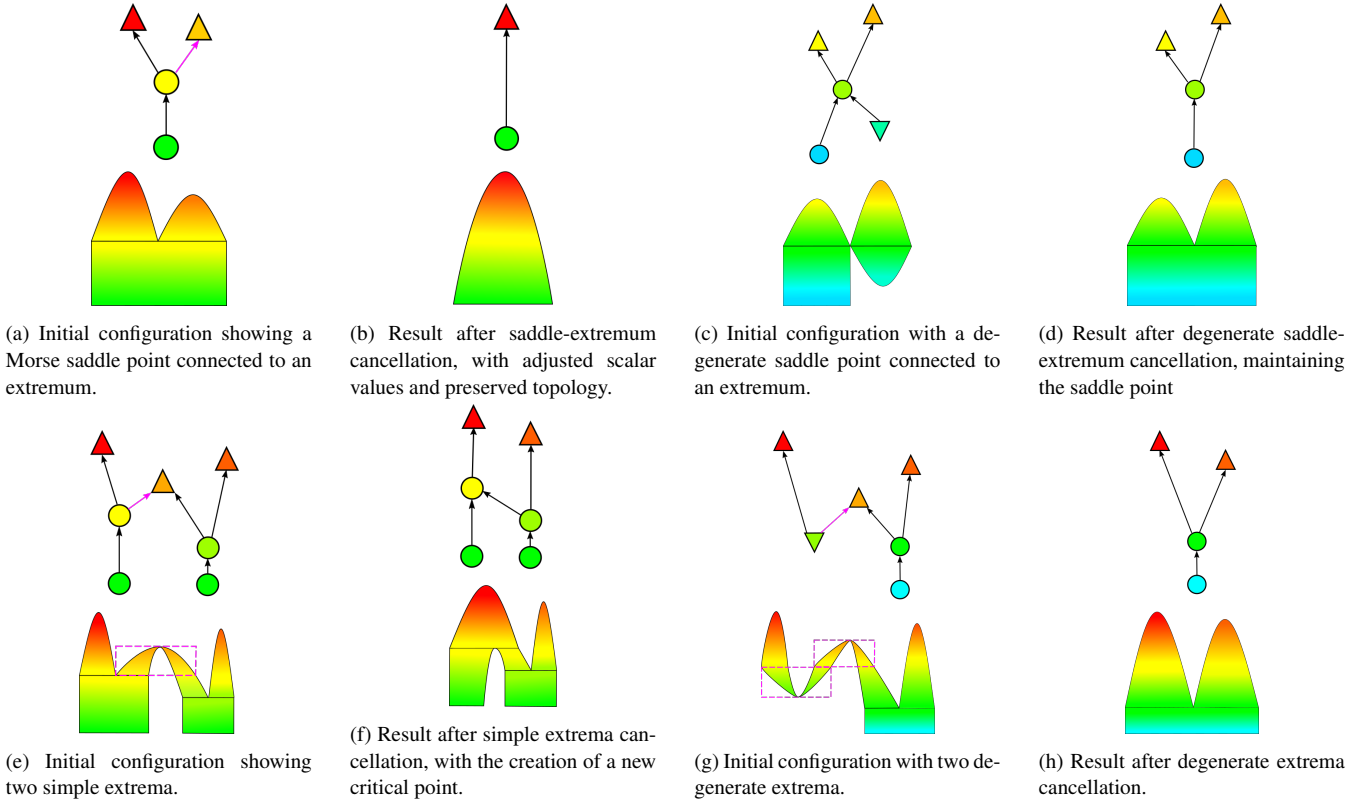


Figure 5: Illustration of critical point cancellation operations showing both Reeb graphs (top) and their corresponding continuous function representations (bottom) before and after cancellation. Colors indicate scalar values from minimum (blue) to maximum (red). Critical points are represented as colored nodes: triangles for extrema and circles for saddle points, with color indicating scalar value. Purple highlights indicate cancellation regions and candidat edges.

of critical points, and its incident edges are merged into a single edge. During this merger, the algorithm maintains the proper ordering of regular vertices along the new edge based on their scalar values.

After each cancellation operation, the algorithm reevaluates all modified edges as potential candidates, as their metrics may have changed. This process continues until no more valid candidates remain or further cancellation would compromise the graph’s essential topology.

Figure 5 illustrates the cancellation operations through four fundamental scenarios. Each scenario is represented through two complementary visualizations: a Reeb graph (top) and its corresponding continuous function representation (bottom). In the Reeb graphs, critical points are depicted as nodes (triangles for extrema, circles for saddle points) with colors indicating scalar values. The continuous representation below each graph shows how the scalar function varies across the domain, with colors transitioning from blue (minimum) through green and yellow to red (maximum). Candidate edges for cancellation are highlighted in purple, and regions affected by the cancellation are indicated by purple dashed boxes.

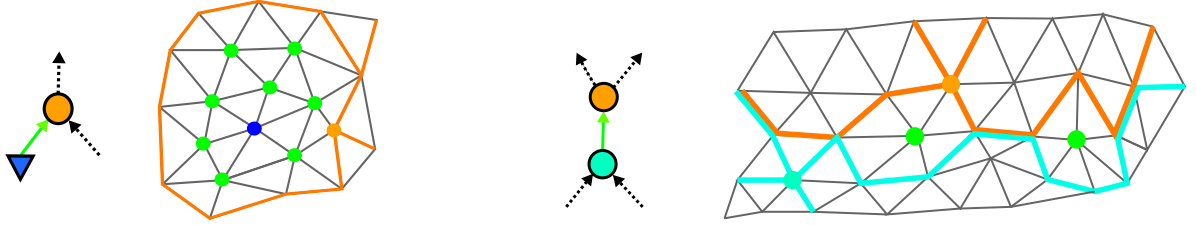
The first scenario (a-b) demonstrates a basic saddle-extremum cancellation. The initial configuration in (a) shows a Morse saddle

point connected to an extremum via a single edge. Following cancellation (b), the algorithm eliminates the extremum while preserving the saddle point and its connections to the broader graph structure. The scalar values of vertices within the affected region are carefully adjusted to maintain smooth transitions in the simplified structure.

The second scenario (c-d) addresses a more complex case: saddle-extremum cancellation involving a degenerate saddle. Beginning with a degenerate saddle connected to an extremum (c), the post-cancellation result (d) successfully maintains the saddle’s intricate connectivity pattern while removing the extremum, demonstrating the algorithm’s ability to handle degenerate critical points.

The third scenario (e-f) explores saddle-extremum cancellation with a degenerate extremum. The post-cancellation configuration (f) shows how the algorithm manages the scalar values of vertices within the highlighted purple region, setting them to match the saddle value. The connection between the green saddle and the yellow node is preserved, effectively smoothing the function while maintaining essential topological features.

The final scenario (g-h) illustrates the cancellation process between two degenerate extrema. From the initial state showing two distinct degenerate extrema (g), the algorithm produces a simplified



(a) A Reeb graph edge (in green) with a minimum node (in blue) and a saddle node (in orange). The discrete outline of both nodes and the set of regular vertices in the edge are highlighted on the mesh.

(b) A Reeb graph edge (in green) with two saddle nodes (in cyan and orange). The discrete outline of both nodes and the set of regular vertices in the edge are highlighted on the mesh.

Figure 6: Two edges of a Reeb graph and their discrete local representation on the mesh.

fied structure (h) that consolidates these extrema into a single node while preserving essential connectivity. The scalar values within the purple regions are carefully adjusted to maintain consistency throughout the affected area, allowing to handle complex degenerate cases while preserving topological integrity.

The algorithm achieves computational efficiency of  $O(e \log e)$ , where  $e$  represents the total number of removed candidate edges, through systematic management of the priority queue structure. This implementation maintains both deterministic execution and topological integrity throughout the simplification process, while the priority-based processing ensures consistent handling of cancellation operations. The method preserves essential topological structures, including handles and tunnels, during the systematic reduction of the Reeb graph complexity. Furthermore, the simplified structure retains precise vertex-graph correspondence and scalar function coherence while preserving critical points and significant topological features. This topologically faithful yet reduced representation provides the foundation for the next region growing phase.

### 3.3. Region growing

After simplifying the Reeb graph through topological cancellation, the purpose of region growing step is to generating meaningful, contiguous segments from the graph structure. While the Reeb graph captures essential topological features, direct segmentation based solely on graph connectivity can lead to disconnected regions, particularly when dealing with scalar functions that exhibit significant local variations, such as curvature-based measures.

A fundamental challenge lies in the nature of vertex connectivity between different types of nodes. For edges connecting an extremum node to a saddle node, the set of regular vertices forms a continuous region on the mesh surface. This continuity exists because a discrete extremum contour and its neighboring contour have adjacent representative vertices on the surface, as illustrated in Figure 6a. However, this property does not hold for edges connecting two saddle nodes, as shown in Figure 6b, where consecutive discrete regular or saddle contours may have non-adjacent representative vertices on the surface. This discontinuity poses particular challenges for traditional Reeb graph-based segmentation methods [TVD07, BDBP09] when applied to scalar functions that gen-

erate numerous critical nodes or when saddle segments fail to form large contiguous sets.

The proposed region growing algorithm addresses these challenges by integrating both topological and geometric connectivity constraints. The algorithm maintains a priority queue of candidate node-region pairs, initially populated with nodes adjacent to extremum points. A Reeb graph node becomes a candidate for addition to a region when it is adjacent in the graph to at least one previously assigned node, ensuring continuous growth through the graph structure.

For each candidate node  $n$  and potential target region  $R$ , the algorithm evaluates their geometric connectivity by defining a boundary set that identifies pairs of adjacent vertices:

$$\text{Boundary}(n, R) = (v, v_r) \mid v \in V(n), v_r \in V(R), v_r \in \text{Adj}(v) \quad (7)$$

where:

- $V(n)$  represents the set of mesh vertices associated with Reeb graph node  $n$
- $V(R)$  represents all mesh vertices currently assigned to region  $R$
- $\text{Adj}(v)$  represents vertices adjacent to  $v$  in the mesh

A candidate node can only be added to a region if their boundary set is non-empty, ensuring geometric continuity in the growing region. For valid candidates, we compute a cost function that combines geometric similarity with topological considerations:

$$\text{Cost}(n, R) = \min_{(v, v_r) \in \text{Boundary}(n, R)} |f(v) - f(v_r)| + \lambda \times 1_{|U_{\text{unassigned}}(n)| > 1} \quad (8)$$

where:

- $U_{\text{unassigned}}(n)$  represents the neighboring nodes of  $n$  in the Reeb graph that haven't been assigned to any region
- $\lambda$  is a penalty parameter that influences region growing behavior at saddle points
- $1_{\cdot}$  is the indicator function

The cost function serves multiple purposes: it ensures topological consistency through the requirement of non-empty boundary sets, maintains geometric continuity through mesh adjacency consideration, and preserves features through the scalar function difference term. Additionally, the  $\lambda$  penalty term allow to manage growth through complex topological features, temporarily increasing the cost of expansion along certain paths to allow balanced region development at junction points. Importantly, adjacent nodes in



the Reeb graph may be assigned to different regions, allowing the segmentation to naturally follow underlying surface features rather than being constrained by graph connectivity alone.

After adding a node to a region, its previously unassigned neighbors become new candidates for region assignment and the algorithm continues iteratively until all nodes have been assigned, with the penalty parameter  $\lambda$  providing control over the balance between compact regions and feature adherence. Through careful implementation of the priority queue and associated data structures, the method achieves  $O(n \log n)$  time complexity, where  $n$  is the number of mesh vertices.

#### 4. Results and discussion

Our experimental results demonstrate the versatility and effectiveness of the proposed mesh segmentation method across different types of input geometry and scalar functions. We present two distinct applications that highlight the method’s adaptability: segmentation of planetary surface features using Shape Index, and part-based decomposition of 3D models using Shape Diameter Function.

##### 4.1. Shape Index

The Shape Index (SI), introduced by [KVD92], represents a quantitative measure for characterizing local surface geometry. This scale-invariant descriptor, derived from principal curvatures, establishes a continuous spectrum of shape classifications that characterizes the transition between concave and convex features.

The Shape Index is defined at each surface point using the maximum ( $\kappa_1$ ) and minimum ( $\kappa_2$ ) principal curvatures through the following formulation:

$$SI = \frac{2}{\pi} \arctan \left( \frac{\kappa_2 + \kappa_1}{\kappa_2 - \kappa_1} \right), \quad \kappa_1 \geq \kappa_2 \quad (9)$$

This formulation maps surface shapes to the interval  $[-1, +1]$ , with specific values corresponding to distinct local surface configurations:  $-1.0$  indicates spherical cup formation (complete concave),  $-0.5$  denotes cylindrical concave features,  $0.0$  represents symmetric saddles or flat surfaces,  $+0.5$  corresponds to cylindrical convex regions, and  $+1.0$  signifies spherical caps (complete convex). [DJ97] subsequently proposed a normalized version mapping to the interval  $[0, 1]$ , facilitating computational implementation while maintaining discriminative capabilities.

The Shape Index manifests several significant properties that establish its utility in surface analysis. Its scale invariance derives from its dependence on principal curvature ratios rather than absolute values, ensuring independence from feature dimensions. The measure exhibits rotation invariance, maintaining constant values under rigid transformations. Furthermore, the sign convention facilitates systematic interpretation of local surface characteristics, with positive values indicating convex regions and negative values denoting concave formations.

Figure 7 presents the implementation of Shape Index-based segmentation on a digital terrain model of the Vesta asteroid surface. The color distribution represents the local surface geometry:

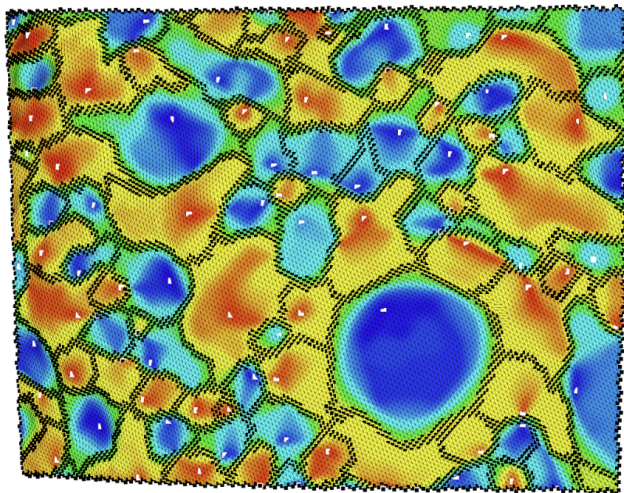


Figure 7: Segmentation results using Shape Index on Vesta asteroid terrain. Colors indicate surface geometry (blue: concave, yellow-green: transitional, red: convex). White dots: Reeb graph critical points. Black lines: segment boundaries.

concave features such as crater floors and depressions appear in blue, transitional regions corresponding to crater walls and gradual slopes manifest in yellow-green, and convex features including crater rims and elevated terrain are depicted in red. The segmentation boundaries and Reeb graph critical points, indicated by black lines and white dots respectively, demonstrate the method’s capacity to capture underlying topological structure.

The segmentation implementation utilizes specific parameter values optimized for crater feature detection while maintaining topological integrity. A separation parameter of 0.1 enables differentiation between distinct crater components while suppressing over-segmentation of minor surface variations. An area ratio threshold of 0.01 facilitates multi-scale feature detection, accommodating both major and minor crater formations. The lambda parameter value of 1.0 implements topological constraints at saddle points during region propagation, ensuring simultaneous development of multiple regions and preventing segmentation dominance by individual regions.

The Shape Index demonstrates particular efficacy in planetary surface analysis through its capacity to characterize local surface geometry independently of absolute elevation. This characteristic proves especially valuable in contexts prioritizing morphological feature identification and classification over absolute height measurements. The integration of Shape Index with Reeb graph topology establishes a methodological framework for automated delineation of impact craters and related geological features across multiple scales, while the implemented parameters ensure both geometric precision and topological consistency in the resultant segmentation.

## 4.2. Shape Diameter Function

The Shape Diameter Function (SDF), introduced by [GSCO07] and further developed by [SSCO08], represents a fundamental volumetric shape descriptor that has demonstrated significant utility in shape analysis and segmentation applications [SSS\*10]. This function establishes a scalar measure derived from the Medial Axis Transform and its associated shape-radius properties, enabling local shape characterization that maintains invariance to pose transformations for closed manifold surfaces.

The computation of the SDF implements a ray-casting methodology that systematically evaluates local volume thickness. For each vertex  $v_i$  on the mesh surface, the algorithm constructs a cone centered on the inward-normal vector  $n_i$ . The measurement process consists of several sequential steps:

$$SDF(v_i) = \frac{\sum_{j=1}^N w_j d_j}{\sum_{j=1}^N w_j} \quad (10)$$

where  $d_j$  represents the ray-intersection distances and  $w_j$  denotes the angular weights. The procedure encompasses:

- Construction of a cone aligned with the inward-normal  $n_i$  at vertex  $v_i$
- Emission of rays within the cone’s angular range from position  $v_i$
- Calculation of distances to valid intersection points, defined as locations where the surface normal orientation is outward
- Computation of a weighted average of the measured distances, with weights inversely proportional to the angle between each ray and the cone’s central axis

The robustness of this descriptor is enhanced through bilateral filtering applied to the vertex’s local neighborhood, mitigating the effects of noise and local geometric irregularities. However, the SDF computation exhibits sensitivity to local geometric references, particularly surface normals and tangent planes. [CLS\*18] addressed these limitations by implementing an improved methodology that utilizes normals computed on an offset surface for more reliable distance measurements.

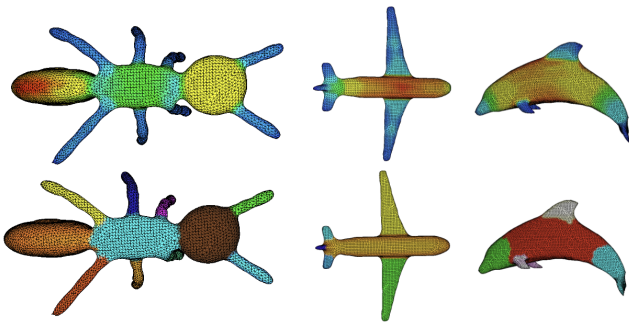


Figure 8: Comparative visualization of Shape Diameter Function analysis. Upper row: SDF scalar field mapping. Lower row: Resultant segmentation using the proposed method. From left to right: arthropod, aircraft, and dolphin models from the Princeton Benchmark dataset.

Figure 8 presents the application of our segmentation methodol-

ogy utilizing SDF as the scalar function on selected models from the Princeton Benchmark dataset. The upper row displays the SDF scalar field mapping, where color variations indicate local shape thickness. The lower row demonstrates the corresponding segmentations derived through our method. The implementation employs specific parameter values optimized for part-based decomposition: a separation threshold of 0.25, an area ratio of 0.1, and a lambda value of 0.4.

The segmentation results demonstrate the method’s capacity to identify semantically meaningful components across diverse object categories. The arthropod model exhibits clear delineation of body segments and appendages, the aircraft model shows distinct separation of primary structural components (fuselage, wings, and tail), and the marine mammal model demonstrates appropriate segmentation of anatomical features. These results validate the effectiveness of combining SDF-based geometric analysis with Reeb graph topological structures for automated part-based decomposition.

For implementation purposes, this study utilizes the SDF computation provided by the CGAL mesh library [YL23], leveraging its robust and optimized implementation. This choice facilitates reproducibility and standardization of the segmentation pipeline, while the method’s modular design permits straightforward integration of alternative scalar functions when required by specific application contexts.

Benchmarks: [CGF09]

Let us now compare our method in the context of the Princeton benchmark. This benchmarking dataset comprises 4,300 manually generated segmentations (created by people from around the world) for 380 surface meshes collected into 19 different object categories. Additionally, the dataset includes a set of segmentations produced by seven algorithms published before 2009, namely, KMeans (hierarchical clustering technique), random walks (iterative clustering technique), fitting primitives (hierarchical clustering technique), randomized cuts (boundary-based technique), core extraction (region growing technique) and also SDF (hierarchical clustering technique).

## 5. Conclusion

The proposed Reeb graph-based mesh segmentation method demonstrates robust and versatile performance across various application domains. By seamlessly integrating topological and geometric analysis, the approach delivers accurate and consistent segmentation results that capture both intrinsic shape features and the underlying structural properties of 3D meshes.

The primary contribution is a unified segmentation framework that effectively combines local geometric features with global topological structures. The algorithm’s ability to accommodate diverse scalar functions, as demonstrated through implementations with Shape Index and Shape Diameter Function, establishes its versatility for chart-based and part-based segmentation tasks. This framework overcomes traditional limitations in Reeb graph-based segmentation by handling both simple and degenerate critical points.

A second contribution is the novel cancellation algorithm that can process degenerate and non-degenerate critical points without

unfolding, while preserving the link between graph nodes and mesh vertices. This approach also serves as an effective smoothing operator for scalar functions.

Computationally, the method achieves optimal efficiency with an overall complexity of  $O(n \log n)$  for a mesh with  $n$  vertices. This performance derives from the integration of Reeb graph construction ( $O(n \log n)$ ), topological simplification ( $O(e \log e)$  for  $e$  removed edges), and region growing ( $O(n \log n)$ ). The use of the Reeb graph as an intermediate representation provides significant computational advantages over direct mesh processing approaches, particularly for large-scale datasets.

The method's effectiveness has been validated through diverse applications, from planetary surface analysis using Shape Index to part-based decomposition using Shape Diameter Function. These results demonstrate the framework's adaptability across domains and its capability to handle varying geometric contexts.

Future research could explore extending the approach to support multivariate Reeb graphs, enabling simultaneous analysis of multiple scalar functions for more sophisticated segmentation criteria. Such an extension, combined with adapted cost functions and clustering techniques, could facilitate advanced applications such as mesh comparison and classification. The present algorithm represents a significant step toward these objectives.

## Acknowledgements

This project has been funded by the Burgundy Regional Council under the contract 2022-Y-14262 "3DKAR".

## References

- [ABS03] ATTENE M., BIASOTTI S., SPAGNUOLO M.: Shape understanding by contour-driven retiling. *The Visual Computer* 19, 2 (2003), 127–138.
- [ACK01] AMENTA N., CHOI S., KOLLURI R. K.: The power crust, unions of balls, and the medial axis transform. *Computational Geometry* 19, 2-3 (2001), 127–153.
- [AFS06] ATTENE M., FALCIDIENO B., SPAGNUOLO M.: Hierarchical mesh segmentation based on fitting primitives. *The Visual Computer* 22 (2006), 181–193.
- [AKM\*06] ATTENE M., KATZ S., MORTARA M., PATANÉ G., SPAGNUOLO M., TAL A.: Mesh segmentation—a comparative study. In *IEEE International Conference on Shape Modeling and Applications 2006 (SMI'06)* (2006), IEEE, pp. 7–7.
- [APP\*07] AGATHOS A., PRATIKAKIS I., PERANTONIS S., SAPIDIS N., AZARIADIS P.: 3d mesh segmentation methodologies for cad applications. *Computer-Aided Design and Applications* 4, 6 (2007), 827–841.
- [ATC\*08] AU O. K.-C., TAI C.-L., CHU H.-K., COHEN-OR D., LEE T.-Y.: Skeleton extraction by mesh contraction. *ACM transactions on graphics (TOG)* 27, 3 (2008), 1–10.
- [AZC\*11] AU O. K.-C., ZHENG Y., CHEN M., XU P., TAI C.-L.: Mesh segmentation with concavity-aware fields. *IEEE Transactions on Visualization and Computer Graphics* 18, 7 (2011), 1125–1134.
- [BA92] BRANDT J. W., ALGAZI V. R.: Continuous skeleton computation by voronoi diagram. *CVGIP: Image understanding* 55, 3 (1992), 329–338.
- [Ban70] BANCHOFF T. F.: Critical points and curvature for embedded polyhedral surfaces. *The American Mathematical Monthly* 77, 5 (1970), 475–485.
- [BAT12] BERGAMASCO F., ALBARELLI A., TORSSELLO A.: A graph-based technique for semi-supervised segmentation of 3d surfaces. *Pattern Recognition Letters* 33, 15 (2012), 2057–2064.
- [BDBP09] BERRETTI S., DEL BIMBO A., PALA P.: 3d mesh decomposition using reeb graphs. *Image and Vision Computing* 27, 10 (2009), 1540–1554.
- [Beu92] BEUCHER S.: The watershed transformation applied to image segmentation. *Scanning microscopy* 1992, 6 (1992), 28.
- [BFS00] BIASOTTI, FALCIDIENO, SPAGNUOLO: Shape abstraction using computational topology techniques. In *International Workshop on Geometric Modelling* (2000), Springer, pp. 209–222.
- [BKS01] BITTER I., KAUFMAN A. E., SATO M.: Penalized-distance volumetric skeleton algorithm. *IEEE Transactions on Visualization and Computer Graphics* 7, 3 (2001), 195–206.
- [Blu67] BLUM H.: A transformation for extracting new descriptions of shape. *Models for the perception of speech and visual form* (1967), 362–380.
- [BP12] BRANDOLINI L., PIASTRA M.: Computing the reeb graph for triangle meshes with active contours. *ICPRAM (2) 12* (2012), 80–89.
- [BPVR11] BENJAMIN W., POLK A. W., VISHWANATHAN S., RAMANI K.: Heat walk: Robust salient segmentation of non-rigid shapes. In *Computer Graphics Forum* (2011), vol. 30, Wiley Online Library, pp. 2097–2106.
- [CCZ07] COUPRIE M., COEURJOLLY D., ZROUR R.: Discrete bisector function and euclidean skeleton in 2d and 3d. *Image and Vision Computing* 25, 10 (2007), 1543–1556.
- [CDST95] CHAZELLE B., DOBKIN D. P., SHOURABOURA N., TAL A.: Strategies for polyhedral surface decomposition: An experimental study. In *Proceedings of the eleventh annual symposium on Computational geometry* (1995), pp. 297–305.
- [CGF09] CHEN X., GOLOVINSKIY A., FUNKHOUSER T.: A benchmark for 3d mesh segmentation. *Acm transactions on graphics (tog)* 28, 3 (2009), 1–12.
- [CLS\*18] CHEN S., LIU T., SHU Z., XIN S., HE Y., TU C.: Fast and robust shape diameter function. *PLOS ONE* 13, 1 (01 2018), 1–18. URL: <https://doi.org/10.1371/journal.pone.0190666>, doi:10.1371/journal.pone.0190666.
- [CSM07] CORNEA N. D., SILVER D., MIN P.: Curve-skeleton properties, applications, and algorithms. *IEEE Transactions on visualization and computer graphics* 13, 3 (2007), 530.
- [DGG03] DEY T. K., GIESEN J., GOSWAMI S.: Shape segmentation and matching with flow discretization. In *WADS* (2003), vol. 3, Springer, pp. 25–36.
- [DJ97] DORAI C., JAIN A. K.: Cosmos—a representation scheme for 3d free-form objects. *IEEE Transactions on Pattern Analysis and Machine Intelligence* 19, 10 (1997), 1115–1130.
- [FKS\*04] FUNKHOUSER T., KAZHDAN M., SHILANE P., MIN P., KIEFER W., TAL A., RUSINKIEWICZ S., DOBKIN D.: Modeling by example. *ACM transactions on graphics (TOG)* 23, 3 (2004), 652–663.
- [FSKR11] FANG Y., SUN M., KIM M., RAMANI K.: Heat-mapping: A robust approach toward perceptually consistent mesh segmentation. In *CVPR 2011* (2011), IEEE, pp. 2145–2152.
- [GF08] GOLOVINSKIY A., FUNKHOUSER T.: Randomized cuts for 3d mesh analysis. In *ACM SIGGRAPH Asia 2008 papers*. 2008, pp. 1–12.
- [GSCO07] GAL R., SHAMIR A., COHEN-OR D.: Pose-oblivious shape signature. *IEEE Transactions on Visualization and Computer Graphics* 13, 2 (Mar. 2007), 261–270. doi:10.1109/TVCG.2007.45.
- [HA03] HÉTROUY F., ATTALI D.: Topological quadrangulations of closed triangulated surfaces using the reeb graph. *Graphical Models* 65, 1-3 (2003), 131–148.
- [HS97] HOFFMAN D. D., SINGH M.: Saliency of visual parts. *Cognition* 63, 1 (1997), 29–78.

- [HSKK01] HILAGA M., SHINAGAWA Y., KOHMURA T., KUNII T. L.: Topology matching for fully automatic similarity estimation of 3d shapes. In *Proceedings of the 28th annual conference on Computer graphics and interactive techniques* (2001), pp. 203–212.
- [KG00] KARNI Z., GOTSMAN C.: Spectral compression of mesh geometry. In *Proceedings of the 27th annual conference on Computer graphics and interactive techniques* (2000), pp. 279–286.
- [Kos03] KOSCHAN A.: Perception-based 3d triangle mesh segmentation using fast marching watersheds. In *2003 IEEE Computer Society Conference on Computer Vision and Pattern Recognition, 2003. Proceedings.* (2003), vol. 2, IEEE, pp. II–II.
- [KT03] KATZ S., TAL A.: Hierarchical mesh decomposition using fuzzy clustering and cuts. *ACM transactions on graphics (TOG)* 22, 3 (2003), 954–961.
- [KVD92] KOENDERINK J. J., VAN DOORN A. J.: Surface shape and curvature scales. *Image and vision computing* 10, 8 (1992), 557–564.
- [LHMR08] LAI Y.-K., HU S.-M., MARTIN R. R., ROSIN P. L.: Fast mesh segmentation using random walks. In *Proceedings of the 2008 ACM symposium on Solid and physical modeling* (2008), pp. 183–191.
- [Llo82] LLOYD S.: Least squares quantization in pcm. *IEEE transactions on information theory* 28, 2 (1982), 129–137.
- [LLS\*05] LEE Y., LEE S., SHAMIR A., COHEN-OR D., SEIDEL H.-P.: Mesh scissoring with minima rule and part salience. *Computer Aided Geometric Design* 22, 5 (2005), 444–465.
- [LV99] LAZARUS F., VERRONST A.: Level set diagrams of polyhedral objects. In *Proceedings of the fifth ACM symposium on Solid modeling and applications* (1999), pp. 130–140.
- [LW08] LAVOUÉ G., WOLF C.: Markov random fields for improving 3d mesh analysis and segmentation. In *3DOR@ Eurographics* (2008), pp. 25–32.
- [LWTH01] LI X., WOON T. W., TAN T. S., HUANG Z.: Decomposing polygon meshes for interactive applications. In *Proceedings of the 2001 symposium on Interactive 3D graphics* (2001), pp. 35–42.
- [LZ04] LIU R., ZHANG H.: Segmentation of 3d meshes through spectral clustering. In *12th Pacific Conference on Computer Graphics and Applications, 2004. PG 2004. Proceedings.* (2004), IEEE, pp. 298–305.
- [LZ07] LIU R., ZHANG H.: Mesh segmentation via spectral embedding and contour analysis. In *Computer Graphics Forum* (2007), vol. 26, Wiley Online Library, pp. 385–394.
- [LZHM06] LAI Y.-K., ZHOU Q.-Y., HU S.-M., MARTIN R. R.: Feature sensitive mesh segmentation. In *Proceedings of the 2006 ACM symposium on Solid and physical modeling* (2006), pp. 17–25.
- [Mil63] MILNOR J. W.: *Morse theory*. No. 51. Princeton university press, 1963.
- [MM02] MISCHAIKOW K., MROZEK M.: Conley index. *Handbook of dynamical systems* 2 (2002), 393–460.
- [MP02] MORTARA M., PATANE G.: Affine-invariant skeleton of 3d shapes. In *Proceedings SMI. Shape Modeling International 2002* (2002), IEEE, pp. 245–278.
- [MPS\*04] MORTARA M., PATANÉ G., SPAGNUOLO M., FALCIDIENO B., ROSSIGNAC J.: Plumber: a method for a multi-scale decomposition of 3 d shapes into tubular primitives and bodies. In *Symposium on Solid Modeling and Applications* (2004), pp. 339–344.
- [MPS06] MORTARA M., PATANÉ G., SPAGNUOLO M.: From geometric to semantic human body models. *Computers & Graphics* 30, 2 (2006), 185–196.
- [MW98] MANGAN A. P., WHITAKER R. T.: Surface segmentation using morphological watersheds. In *Proc. IEEE Visualization* (1998).
- [NGH04] NI X., GARLAND M., HART J. C.: Fair morse functions for extracting the topological structure of a surface mesh. *ACM Transactions on Graphics (TOG)* 23, 3 (2004), 613–622.
- [Par12] PARSA S.: A deterministic  $o(m \log m)$  time algorithm for the reeb graph. In *Proceedings of the twenty-eighth annual symposium on Computational geometry* (2012), pp. 269–276.
- [PSG\*06] PODOLAK J., SHILANE P., GOLOVINSKIY A., RUSINKIEWICZ S., FUNKHOUSER T.: A planar-reflective symmetry transform for 3d shapes. In *ACM SIGGRAPH 2006 Papers.* 2006, pp. 549–559.
- [Pud98] PUDNEY C.: Distance-ordered homotopic thinning: a skeletonization algorithm for 3d digital images. *Computer vision and image understanding* 72, 3 (1998), 404–413.
- [RMG15] RODRIGUES R. S., MORGADO J. F., GOMES A. J.: A contour-based segmentation algorithm for triangle meshes in 3d space. *Computers & Graphics* 49 (2015), 24–35.
- [RMG18] RODRIGUES R. S., MORGADO J. F., GOMES A. J.: Part-based mesh segmentation: a survey. In *Computer Graphics Forum* (2018), vol. 37, Wiley Online Library, pp. 235–274.
- [Sha08] SHAMIR A.: A survey on mesh segmentation techniques. In *Computer graphics forum* (2008), vol. 27, Wiley Online Library, pp. 1539–1556.
- [SKK91] SHINAGAWA Y., KUNII T. L., KERGOSIEN Y. L.: Surface coding based on morse theory. *IEEE computer graphics and applications* 11, 05 (1991), 66–78.
- [SLSK07] SHARF A., LEWINER T., SHAMIR A., KOBELT L.: On-the-fly curve-skeleton computation for 3d shapes. In *Computer Graphics Forum* (2007), vol. 26, Wiley Online Library, pp. 323–328.
- [SSCO08] SHAPIRA L., SHAMIR A., COHEN-OR D.: Consistent mesh partitioning and skeletonisation using the shape diameter function. *The Visual Computer* 24 (2008), 249–259.
- [SSS\*10] SHAPIRA L., SHALOM S., SHAMIR A., COHEN-OR D., ZHANG H.: Contextual part analogies in 3d objects. *International Journal of Computer Vision* 89, 2-3 (Sept. 2010), 309–326. doi: 10.1007/s11263-009-0279-0.
- [STK02] SHLAFMAN S., TAL A., KATZ S.: Metamorphosis of polyhedral surfaces using decomposition. In *Computer graphics forum* (2002), vol. 21, Wiley Online Library, pp. 219–228.
- [SWG\*03] SANDER P. V., WOOD Z. J., GORTLER S., SNYDER J., HOPPE H.: Multi-chart geometry images.
- [TPT15] THEOLOGOU P., PRATIKAKIS I., THEOHARIS T.: A comprehensive overview of methodologies and performance evaluation frameworks in 3d mesh segmentation. *Computer Vision and Image Understanding* 135 (2015), 49–82.
- [TVD07] TIERNY J., VANDEBORRE J.-P., DAOUDI M.: Topology driven 3d mesh hierarchical segmentation. In *IEEE International Conference on Shape Modeling and Applications 2007 (SMI'07)* (2007), IEEE, pp. 215–220.
- [TVD09] TIERNY J., VANDEBORRE J.-P., DAOUDI M.: Partial 3d shape retrieval by reeb pattern unfolding. In *Computer Graphics Forum* (2009), vol. 28, Wiley Online Library, pp. 41–55.
- [WLAT14] WANG H., LU T., AU O. K.-C., TAI C.-L.: Spectral 3d mesh segmentation with a novel single segmentation field. *Graphical models* 76, 5 (2014), 440–456.
- [WML\*06] WU F.-C., MA W.-C., LIANG R.-H., CHEN B.-Y., OUHYOUNG M.: Domain connected graph: the skeleton of a closed 3d shape for animation. *The Visual Computer* 22 (2006), 117–135.
- [XSW03] XIAO Y., SIEBERT P., WERGHEN N.: A discrete reeb graph approach for the segmentation of human body scans. In *Fourth International Conference on 3-D Digital Imaging and Modeling, 2003. 3DIM 2003. Proceedings.* (2003), IEEE, pp. 378–385.
- [YL23] YAZ I. O., LORIOT S.: Triangulated surface mesh segmentation. In *CGAL User and Reference Manual*, 5.6 ed. CGAL Editorial Board, 2023. URL: <https://doc.cgal.org/5.6/Manual/packages.html#PkgSurfaceMeshSegmentation>.

- [YLY\*16] YUAN Q., LI G., XU K., CHEN X., HUANG H.: Space-time co-segmentation of articulated point cloud sequences. In *Computer Graphics Forum* (2016), vol. 35, Wiley Online Library, pp. 419–429.
- [ZH04] ZHOU Y., HUANG Z.: Decomposing polygon meshes by means of critical points. In *10th International Multimedia Modelling Conference, 2004. Proceedings.* (2004), IEEE, pp. 187–195.
- [ZL\*05] ZHANG H., LIU R., ET AL.: Mesh segmentation via recursive and visually salient spectral cuts. In *Proc. of vision, modeling, and visualization* (2005), Citeseer, pp. 429–436.
- [ZLG\*15] ZHANG H., LI C., GAO L., LI S., WANG G.: Shape segmentation by hierarchical splat clustering. *Computers & Graphics* 51 (2015), 136–145.
- [ZLXH08] ZHANG X., LI G., XIONG Y., HE F.: 3d mesh segmentation using mean-shifted curvature. In *Advances in Geometric Modeling and Processing: 5th International Conference, GMP 2008, Hangzhou, China, April 23-25, 2008. Proceedings 5* (2008), Springer, pp. 465–474.
- [ZTS02] ZUCKERBERGER E., TAL A., SHLAFMAN S.: Polyhedral surface decomposition with applications. *Computers & Graphics* 26, 5 (2002), 733–743.
- [ZZWC12] ZHANG J., ZHENG J., WU C., CAI J.: Variational mesh decomposition. *ACM Transactions on Graphics (TOG)* 31, 3 (2012), 1–14.